Accepted Manuscript

Title: CO_2 reduction by C_3N_4-TiO_2 Nafion photocatalytic membrane reactor as a promising environmental pathway to solar fuels

Authors: Adele Brunetti, Francesca Rita Pomilla, Giuseppe Marcì, Elisa Isabel Garcia-Lopez, Enrica Fontananova, Leonardo Palmisano, Giuseppe Barbieri

PII: S0926-3373(19)30518-1
DOI: https://doi.org/10.1016/j.apcatb.2019.117779
Article Number: 117779

Reference: APCATB 117779

To appear in: *Applied Catalysis B: Environmental*

Received date: 1 April 2019
Revised date: 16 May 2019
Accepted date: 25 May 2019

Please cite this article as: Brunetti A, Pomilla FR, Marcì G, Garcia-Lopez EI, Fontananova E, Palmisano L, Barbieri G, CO_2 reduction by C_3N_4-TiO_2 Nafion photocatalytic membrane reactor as a promising environmental pathway to solar fuels, *Applied Catalysis B: Environmental* (2019), https://doi.org/10.1016/j.apcatb.2019.117779

CO_2 reduction by C_3N_4-TiO_2 Nafion photocatalytic membrane reactor as a promising environmental pathway to solar fuels

Adele Brunetti,[1] Francesca Rita Pomilla,[1,2,3] Giuseppe Marcì,[3] Elisa Isabel Garcia-Lopez,[4] Enrica Fontananova,[1] Leonardo Palmisano,[3] Giuseppe Barbieri[1,]*

[1] *Institute on Membrane Technology (ITM-CNR), National Research Council c/o the University of Calabria, Cubo 17C, Via Pietro Bucci, 87036 Rende CS, Italy.*

[2] *Department of Environmental and Chemical Engineering, the University of Calabria Via Pietro Bucci, 87036 Rende CS, Italy*

[3] *Department of Engineering, Università di Palermo, Viale delle Scienze, 90128 Palermo, Italy*

[3] *Department of Biological, Chemical and Pharmaceutical Sciences and Technologies, Università di Palermo, Viale delle Scienze, 90128 Palermo, Italy*

Author whom correspondence should be addressed: g.barbieri@itm.cnr.it

Graphical Abstract

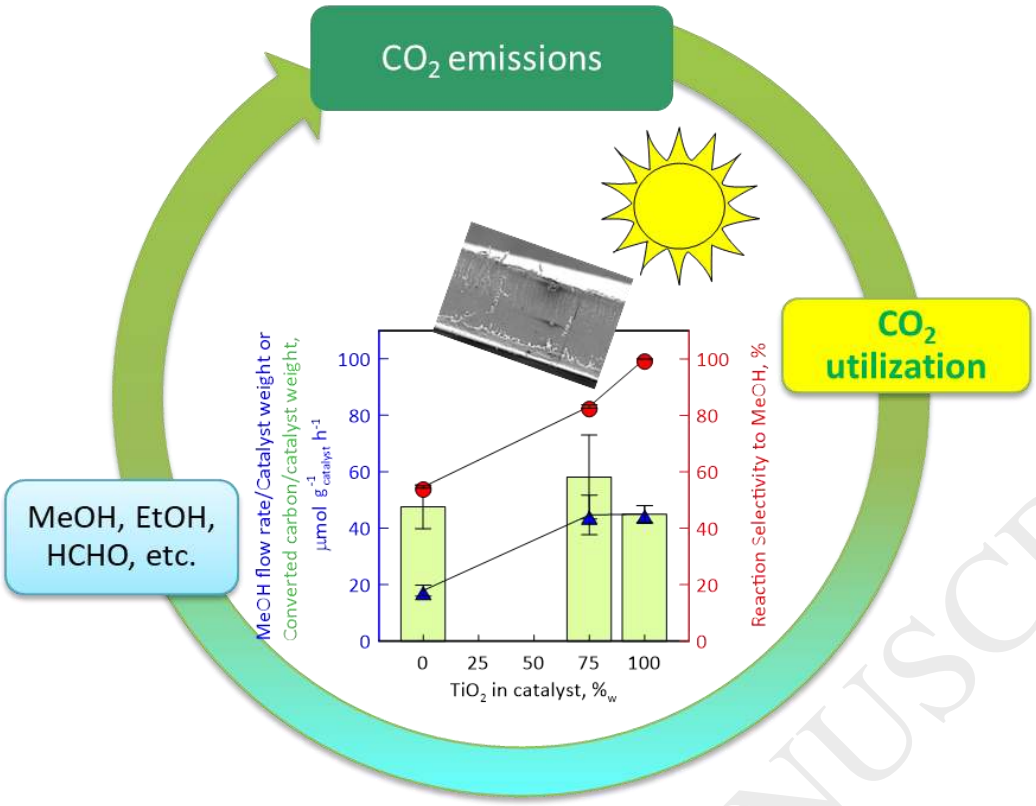

Abstract

We investigated CO_2 photocatalytic reduction coupling, for the first time in literature, the assets offered by the continuous operating mode using C_3N_4-TiO_2 photo-catalyst embedded in a dense Nafion matrix. The reactor performance was analyzed under UV-Vis light in terms of productivity, selectivity and converted carbon. Reaction pressure was specifically investigated for its effect as a "driver" in determining reactor performance, modulating products removal from the reaction volume. In addition, the membrane reactor performance was explored as a function of H_2O/CO_2 feed molar ratio and contact time. The higher feed pressure (5 bar) led to a lesser MeOH production and a greater amount of HCHO, owing to a hindered desorption, which promoted partial oxidation reactions. Total converted carbon instead did not vary significantly with reaction pressure. Membrane reactor with C_3N_4-TiO_2 photocatalyst resulted more performant than other photocatalytic membrane reactors in terms of carbon converted (61 µmol $g_{catalyst}^{-1}$ h^{-1}).

Introduction

The energy strategy, e.g., of the European Union for 2030 and 2050 fixes specific targets for a gradual transition from the current energy system towards a low carbon one, aiming at decreasing Greenhouse Gas emissions in the environment, improving energy efficiency and increasing the use of renewable energy sources.1 Although utilization of CO_2 is not new, as it is used for Enhanced Oil Recovery in the US since the 1970s, it is only until recently that the development of different forms and ways to utilize CO_2 got raising interest. Although it is difficult to assess the market of CO_2 reuse precisely, the classic industrial utilization of CO_2 was estimated to 153 Mton worldwide (40 Mton of which for enhanced hydrocarbon recovery) in 2008, which represents 0.5% of yearly global emissions.2 The main challenge in reducing CO_2 emissions consists in finding new applications beyond the 153 Mton reused today; particularly *via* new technologies which could develop into bigger scale processes whilst ensuring they remain profitable and positive for the environment. For instance, synthesizing energy products could ultimately use 5 to 10% of world emissions, i.e. between 1.5 and 3Gt of CO_2 – ten times more than the amount of CO_2 currently used.[2] Renewable solar energy is used to harness the sun energy and convert it into usable products through solar heating, photovoltaics, thermal electricity, and architecture, and artificial photosynthesis.3,4,5 Photocatalytic transformation of CO_2 into solar fuels is more sustainable, green and favourable than other technologies because of zero additional energy consumption and environmental deterioration.

Nowadays, various semiconductors such as metal oxides, sulphides, graphene-based materials, are explored to act as CO_2 reduction photo-catalysts.6 Among those photocatalysts, TiO_2 is the most extensively investigated UV-light-responsive photo-catalyst because of its exceptional properties such as high chemical stability, low cost, easy availability, and suitable band alignment to CO_2 reduction and water redox potentials.7,8,9,10,11,12,13 Despite these advances, the use of TiO_2 for photocatalytic CO_2 reduction is limited owing to its large band gap, the fast recombination rates of photo-generated charges, and low CO_2 adsorption capacity.14,15

Graphite carbon nitride (g-C_3N_4), possessing a two-dimensional (2D) nanosheet structure like graphene, has recently attracted much attention. The basic skeleton structure of g-C_3N_4 consists of tri-s-triazine units connected with tertiary amino groups, which owns regularly distributed triangular water-selective permeation nanopores throughout the entire laminar structure.[16,17] Moreover, the spacers between the g-C_3N_4 nanosheets, which interact with each other through weak van der Waals forces, also provide nanochannels for water transport while bigger molecules are retained.[18,19] Owing to this unique nanosheet structure, g-C_3N_4 exhibited many useful properties with applications in many fields, such as materials for membrane separation,[20,21] photocatalysis,[22,23,24] and electronic devices.[25] g-C_3N_4 shows other advantages for CO_2 photo-reduction because it is rich of N basic sites, which favour the CO_2 adsorption step. Because of these outstanding properties, several reports were published on different synthetic strategies affording specific crystal phase, surface area, energy bands position and band gap energy.[26,27]

The synthesis of composite hybrid materials was explored to improve photocatalytic activity, taking advantage of the complementary features of inorganic and organic photocatalysts.[28] Composites of g-C_3N_4 and TiO_2 have shown superior photocatalytic activity by the formation of an artificial photocatalytic Z-scheme.[29,30,31] They were used for various applications including CO_2 reduction.[32,33,34,35] Very recently, Petit et al.,[28] reported on the use, for the first time, of TiO_2/C_3N_4 nanosheet nanocomposites for CO_2 photoreduction under UV-visible irradiation using H_2 as sacrificial agent, demonstrating that the photocatalytic reduction of CO_2 could be improved greatly by forming composite materials with increased CO_2 adsorption capacity and which can suppress electron-hole recombination by facilitation of charge transfer.

On the basis of these results, in this work g-C_3N_4 was successfully coupled with TiO_2 to promote CO_2 photo-reduction in a photocatalytic membrane reactor. TiO_2 is selected to afford the hard water oxidation semi-reaction (+1.23 eV vs SHE) being the C_3N_4 valence band just enough positive to drive it (+1.5 eV vs SHE). TiO_2 has, in fact, a greater band gap (ca. 3.0 eV),[34] even though a less negative conduction band (-0.3 eV), [34] thus less tendency to reduce CO_2. By a favoured H_2O reaction with the

photogenerated h^+, the free H^+ ions required for CO_2 reduction semi-reaction are available. The coupling of these two catalysts promotes CO_2 conversion, enhancing the composite capability in terms of H_2O oxidation and CO_2 reduction.[36,37,38]

We already demonstrated the advantage offered by the use of a photocatalytic membrane reactor operated in continuous with respect to a traditional batch reactor.[39,40] The immobilization of catalyst into polymeric membrane supports and, thus, the use of the membrane as a "mirror" and a contactor significantly enhanced the mass transfer rate of CO_2 and offered the better exposition of catalyst surface area to reactants and light. Further advantages offered by membrane reactor use are the tuning of contact between reactants and catalyst, the reduction of catalyst particles aggregation, an easier recovery of the catalyst which can be simply reused, and a better control of fluid-dynamics.

We used home-made dense mixed matrix TiO_2-based Nafion[39] and C_3N_4-Nafion[40] membranes in photocatalytic reactors operated in continuous for CO_2 photo-reduction.

By comparing these works with the data reported for batch systems, the advantage offered by the continuous system was confirmed, obtaining a MeOH production higher than most of the ones obtained by using simple C_3N_4 or TiO_2 as catalyst and higher or, at least, comparable when it is used as co-catalyst in batch conditions. Moreover, it is worth noticing that differently from what can be found in most of the literature for batch reactors, continuous photocatalytic reactors did not show the production of neither CH_4 nor CO. The synergic effect of the use of a photocatalytic membrane and a continuous flow mode reactor allows the substrate to undergo a lower degree of reduction as fresh CO_2 is continuously fed into the system and the produced species are continuously removed from the catalytic sites, reducing the possibility of having over-oxidation.[39,40]

A key role was played by the continuous operating mode of the photocatalytic reactor which allowed a continuous removal of products from the reaction volume, promoting conversion and depleting side and oxidation reactions. Contact time and feed molar ratio played a primary role in determining

reactor performance, allowing the opportune modulation of products removal from the reaction volume, depleting undesired side and secondary reactions. Nafion, operating similarly to a support in heterogenous catalysis, significantly changes the microenvironment around the photocatalyst particle: it favours CO_2 and H_2O molecules adsorption, driving the adsorbed molecules towards the catalyst. The most significant contribution, beyond the previous one, is the membrane functionality, which changes the flow-path followed by reactants and products from one membrane surface to the other membrane side. This changes significantly the weight of the different elementary reaction steps and leads to a different products distribution.

Inspired by these findings, in this work we report on the reduction of CO_2 to fuels in a continuous photocatalytic membrane reactor equipped with a Nafion membrane with embedded exfoliated C_3N_4-TiO_2. It is a relevant advancement with respect to the previous works, as it couples the assets offered by the continuous operating mode with the use of an enhanced photocatalyst (C_3N_4-TiO_2) directly embedded in a dense polymer matrix. Feed pressure effect was specifically investigated for the first time in literature. This parameter is, in fact, well known as a "driver" in determining reactor performance, allowing the opportune modulation of contact between reactants and catalyst as well as products removal from the reaction volume. In addition, the membrane reactor performance was explored as a function of H_2O/CO_2 feed molar ratio and contact time, both variables having a primary role in the attainment of a much more efficient and selective conversion process.

Materials and Methods

Materials

Nafion™ 5 wt.% solution was purchased from Quintech e.K. – Brennstoffzellen Technologie, Germany. Melamine ($C_3H_6N_6$, 99.0%), methanol (anhydrous 99.8%), absolute ethanol (reagent ISO, reagent Pharmacopoeia European, ≥99.8%), acetone (analytical standard) and formaldehyde (absolute, reagent ISO, reagent Pharmacopoeia European ≥99.8%) were purchased from Sigma-Aldrich, while TiO_2 (P25) (100%) from Evonik. All chemicals were used as received without any further

purification. CO_2 (5.0) was purchased from Sapio srl (Italy). Water used throughout the experiments was purified by means of a Milli-Q system.

All the details on catalyst and catalytic membrane preparation and characterization can be found in the Supplementary Information.

Photocatalytic membrane reactor set-up

C_3N_4-TiO_2/Nafion membrane was assembled in a stainless-steel module (membrane reactor) equipped with a quartz window allowing UV-Visible irradiation. The membrane exposed surface area, allowed by this membrane reactor, is 4.1 cm^2.

The membrane reactor mainly consists of three parts: the catalytic membrane, the feed/retentate chamber and the permeate chamber. The membrane module was placed in such a way that the membrane was in a vertical position to facilitate permeate and retentate sampling of liquid fuels, as well as avoiding stagnant zones. The membrane was irradiated by a medium–high mercury vapor pressure lamp (Zs lamp, Helios Ital quartz, Milan) with emittance from 360 nm (UV-Vis) to 600 nm. The membrane module was continuously fed with CO_2 by means of a mass flow controller, and H_2O fed by means of an HPLC pump, to properly control the feed molar ratio. H_2O was, then, partially vaporized before entering the module by means of an heating coil placed in the exposition chamber. We obtained a multiphase condition with the gaseous phase constituted by CO_2 and part of H_2O, the rest of this latter being in liquid phase.

A reaction pressure of 3 and 5 bar was regulated by a back-pressure controller. The permeate and retentate streams outgoing from the reactor were cooled with apposite ice traps to condense the liquid fraction. The remaining gaseous fraction was then measured by bubble soap flow-meters, (Figure 1). The composition of these gaseous streams was measured by an Agilent Technologies 7890A gas chromatograph with two TCDs and two parallel analytical lines

directly connected to retentate and permeate streams. Each line was equipped with two columns: an HP-Plot-5A, to separate permanent gases such as H_2, O_2, N_2, CH_4 and CO (detection limit=100ppm) and an HP-Poraplot Q, for other species, such as CO_2, C_2H_4, C_2H_6, etc. (detection limit=100ppm).

Table 1 – Operating conditions for reaction experiments

CO_2 flow rate, mL(STP*) min^{-1}	17.5; 30
H_2O/CO_2 feed molar ratio	0.5; 2; 5
Feed/Reaction Pressure, bar	3; 5
Permeate Pressure, bar	1
Contact time, s	2; 3.5
*STP - standard temperature and pressure: 0°C and 1 bar	

The concentration of oxygen obtained as oxidation product of the various reactions is very low and below the impurity contained, e.g., in CO_2 cylinder; therefore, it was not measured. The condensate fraction of the retentate and permeate, periodically sampled, was analysed by an Agilent 6890N gas chromatograph with FID and an HP-5 column. It has to be highlighted that all the measurements, lasting 25-30 h, were performed under a steady state condition, which was reached within 5 h for all the species.

Table 1 summarizes the operating conditions used for photocatalytic measurements. As aforementioned, the performance of photocatalytic membrane reactor was evaluated, among the others, also as a function of the contact time, which was defined accordingly to (eq. 1) referring to the weight of catalyst dispersed in the membrane and CO_2 feed flow rate at STP condition. Therefore, the CO_2 feed flow rate is the same at the same contact time independently of pressure and temperature. The CO_2 was considered as the limiting reagent. No difference in CO_2 exiting the reactor from the feed one could be measured practically; therefore, CO_2 conversion did not represent an appreciable value to be considered significant in order to evaluate the reactor performance. Instead, it was evaluated through the produced species flow rate/catalyst weight (eq. 2), the total converted carbon/catalyst weight ratio (eq. 3), and reaction selectivity (eq. 4).

$$Contact\ time = \frac{Catalyst\ weight\ embedded\ in\ the\ membrane}{CO_2\ feed\ flow\ rate\ [at\ STP]}, s \quad \text{eq. 1}$$

$$\frac{Produced\ species\ flow\ rate}{Catalyst\ weight} = \frac{Compound\ flow\ rate}{Amount\ of\ catalyst\ dispersed\ in\ membrane}, \frac{\mu mol}{h\ g_{catalyst}}$$

eq. 2

$$\frac{Converted\ carbon}{Catalyst\ weight} = \frac{\sum Carbon\ flow\ rate\ for\ each\ produced\ species}{Amount\ of\ catalyst\ dispersed\ in\ membrane}, \frac{\mu mol}{h\ g_{catalyst}}$$

eq. 3

$$Reaction\ Selectivity_i = \frac{i-species\ flow\ rate}{\sum_i^n species\ flow\ rate}, - \quad \text{eq. 4}$$

The catalytic membrane underwent a cleaning procedure before starting photocatalytic reaction measurements to remove any residuals solvent and other low molecular weight organics possibly present in the polymer solution that, otherwise, could be released during the reaction measurements invalidating the results. The membrane cleaning, carried out using the membrane reactor set up used for reaction experiments, consists in subjecting the membrane to a "blank reaction" procedure, where an argon stream is fed together with H_2O to the reactor instead of CO_2, at the same operating condition chosen for the catalytic experiment including light irradiation. It lasted 70 h.

The species distribution as a function of time on stream confirms the presence of MeOH, EtOH, HCHO and acetone at the reactor exit, which decreased along with the time (Figure 2). After about 55 h, no species were longer detected at the reactor outlet. This treatment was protracted for further 14 h for confirming the absence of the various species and, therefore, their nature as residues. The membrane was "cleaned" , therefore the species measured in reaction experiments could only be attributed to the photocatalytic activity of the membrane. The cleaning procedure, in which Ar was fed instead of CO_2 for about 70 hours, confirmed (Figure 2) the absence of CO_2 in the photocatalytic system; in fact, any MeOH, EtOH, or

HCHO, etc. was produced. The stability and reproducibility of reaction measurements confirmed the absence of any Nafion volatilization or C_3N_4 decomposition. As mentioned in our previous work,[38] Nafion (in membrane shape) is the most used polymer in polymer electrolyte membrane fuel cells, which usually operate for really long-time (tens thousands hours) up to 80°C, although other measures were carried up to 140°C. That confirms the long-term stability of Nafion under heating and in presence of water vapour. Similar resistance is expected in the photocatalytic applications under visible/UV light irradiation. We excluded photo-catalyst decomposition since the amount of C_3N_4 present in the membrane is such that, assuming that everything could have degraded, it could have led to a total converted carbon of about 7.5 micromoles, with relevant variations in stability and reproducibility of reaction measurements. More than 150 micromoles of converted carbon were measured in the whole experiments period. The experimental campaign lasted around 160 h. Each measure was repeated along this period to check reproducibility and stability, and no performance change was observed.

Results and discussion

The distribution and the amount of species produced by photocatalytic reaction strongly depends on H_2O/CO_2 feed molar ratio (Figure 3). A high formation of methanol prevails on the other reaction products, at a high H_2O/CO_2 feed molar ratio, reaching 44.7 μmol $g_{catalyst}^{-1}$ h^{-1}, and corresponding to a selectivity of about 83%. A low feed molar ratio instead leads to a wider species distribution. In particular for a H_2O/CO_2 feed molar ratio of 0.5, even though MeOH selectivity is still above 40% with a production rate of 1.7 μmol $g_{catalyst}^{-1}$ h^{-1}, ethanol and acetone are present, showing a reaction selectivity towards these species of 23.4 and 32.8%, respectively. However, the total converted carbon/catalyst weight, which is a measure of the capability of the system to convert CO_2 into other carbon-containing species, is quite modest,

being below 10 μmol $g_{catalyst}^{-1}$ h^{-1}. It means that the high feed molar ratio promotes the methanol selectivity production, as confirmed by a total carbon converted of 58.2 μmol $g_{catalyst}^{-1}$ h^{-1} measured at a feed molar ratio of 5. This trend can be explained by the following (not-elementary) reactions:

$$CO_2 + 2\ H_2O = CH_3OH + 3/2\ O_2 \qquad \text{eq. 5}$$

$$2\ CO_2 + 3\ H_2O = CH_3CH_2OH + 3\ O_2 \qquad \text{eq. 6}$$

$$CO_2 + H_2O = HCHO + O_2 \qquad \text{eq. 7}$$

At a H_2O/CO_2 feed molar ratio of 5 MeOH is the main product (eq. 5), as already observed in previous works.[41,42,43] The formation of acetone and ethanol, in water defect, can be explained considering the occurrence of side reactions of intermediates such as HCHO (eq.7).

Oxygen is one of the oxidation product as foreseen by reactions (Eq. 5, 6 and 7). HCHO, another oxidation product, before leaving the catalytic site reacts (eqs. 8-9)[37] with CH_3OH.

In an open flow system, such as a continuous membrane reactor, any species and also the oxygen is transported far from the reaction volumes (on both retentate and permeate chambers). Thus, the concentrations of the reaction products are lowered by continuous removal and no accumulation (increase) takes place in a steady state. The concentration of some species can be very low and might happen, as for oxygen, to be under detection limit of our apparatus. The steady state requires that the concentration of all the species are constant in time in both membrane reactor chambers; they are measured sampling the respective exiting permeate and retentate streams. The dynamics of elementary reactions step involving oxygen or oxygen-semiconductor interactions cannot produce a net oxygen amount to give a measurable concentration of it with our apparatus.

$$CH_3OH + HCHO + 2\ H^+ + 2\ e^- = C_2H_5OH + H_2O \qquad \text{eq. 8}$$

$2\ CH_3OH + HCHO = CH_3COCH_3 + 2\ H_2O$ eq. 9

Similar trends were obtained at a contact time of 3.5 s (Figure 4), where MeOH was still the favoured product at a high H_2O/CO_2 feed molar ratio. However, the total converted carbon was less than a half of that obtained at a contact time of 2 s.

Analogously, acetone was present at a low feed molar ratio as the reaction selectivity shows; 3.93 $\mu mol\ g_{catalyst}^{-1}\ h^{-1}$ HCHO were formed at a feed molar ratio of 5, to which corresponds a reaction selectivity close to 20%. In any case, the catalyst was highly selective toward MeOH and this can be attributed to the presence of TiO_2, which in our previous work exhibited a full selectivity toward MeOH.[39]

As it is evident by comparing the results reported in Figures 3 and 4, the contact time significantly influences the product distribution and the amount of carbon converted. A preferential formation of MeOH to the other species corresponds at the lowest contact time (Figure 5). MeOH amount decreases in favour of other species such as HCHO as contact time increases. A high contact time, in fact, corresponds to a slower removal of the reaction mixture from reaction volume. This can induce MeOH to be partially oxidized producing formaldehyde (eq. 10) or fully oxidized to CO_2 as reaction product. On the contrary, a low contact time implies a fast product removal from the reaction volume exposed to the light and, thus, a less promotion of side reactions.

$CH_3OH + 1/2\ O_2 = HCHO + H_2O$ eq. 10

The dependence of membrane reactor performance on the contact time is well highlighted in Figure 6 in terms of total converted carbon per gram of catalyst, as an indication of the capability of the system to convert CO_2 into other carbon-containing species.

A high contact time was traduced in a less performant reactor, in fact, the converted carbon is twice at 2 s. The highest conversion of 58.2 μmol $g_{catalyst}^{-1}$ h^{-1} (which corresponds to a quantum efficiency of 0.06%) occurred at the lowest contact time and the highest H_2O/CO_2 feed molar ratio. Moreover, converted carbon tended to increase quite linearly with the feed molar ratio. This increase, much higher at a lower contact time, could be owed to the less significant occurrence of side reactions. Reaction pressure is another parameter, which most often affects the performance of a membrane reactor through reactant adsorption and product desorption. In this view, we explored reactor performance at 5 bar of reaction pressure, fixing the feed molar ratio and contact time that provided the best performance at 3 bar (Figure 7).

MeOH and HCHO resulted the unique products at these new conditions, with a lower amount of MeOH and a greater amount of HCHO with respect to the results obtained at 3 bar. This behaviour can find an explanation in a hindered desorption induced by the higher reaction pressure, which leads to partial oxidation reactions and, thus, to the formation of HCHO to the detriment of MeOH. Total converted carbon resulted really close to that obtained at 3 bar, indicating that the system capability of converting carbon does not change significantly at 5 bar. Even though the reaction is thermodynamically favoured by pressure owing to a reduction in mole number, this positive effect is counterbalanced by difficulties in desorption, which leads to a reduced advantage on total conversion. The reaction is, thus, less selective toward alcohols, passing from 90.8% at 3 bar to 55.1% at 5 bar, whereas it is preferentially selective toward HCHO with a selectivity of 44.6%, five times higher than that obtained at 3 bar (Table 2).

Table 2 – Reaction Selectivity of the various products at a reaction pressure of 3 and 5 bar. (@H_2O/CO_2 feed molar ratio=5 and contact time = 2s).

Species	**Reaction selectivity, %**	
	3 bar	**5 bar**
MeOH	83.2±0.64	54.9±1.0
EtOH	7.6±0.36	0.25±0.01
Total (alcohols)	90.8±1	55.1±1.01

Acetone	0.31±0.02	0.27±0.008
HCHO	8.9±0.024	44.6±0.52

Comparison with other photocatalytic membrane reactors

In our previous works, we studied the CO_2 reduction in photocatalytic membranes reactor by using a TiO_2/Nafion membrane[39] and a C_3N_4/Nafion membrane.[40] In this work, we used the same system with a C_3N_4-TiO_2 catalyst embedded in Nafion as a new photocatalytic membrane. Table 3 summarizes the weight composition of the three membranes investigated.

Table 3– Photocatalytic Membranes – Catalysts content.

Membranes	**TiO_2, wt.%**	**C_3N_4, wt. %**	**TiO_2:C_3N_4 wt.%**	**Thickness µm**	**Ref.**
C_3N_4/Nafion	0	1.2	0:100	65± 1	[40]
C_3N_4-TiO_2/Nafion	0.9	0.3	75:25	78 ± 7	This work
TiO_2/Nafion	1.2	0	100:0	59 ± 0.2	[39]

Three different contents of the two photocatalytic phases are, here, compared: pure TiO_2, pure C_3N_4 and a mixture TiO_2:C_3N_4=25:75 wt.%. This ratio was selected for having the same surface area extension for both C_3N_4 and TiO_2, which have a specific surface area of 154 and 50 $m^2 g^{-1}$, respectively. Figure 8 shows a comparison of the results obtained with the two membranes containing C_3N_4 at a contact time of 2 s and 3 bar of reaction pressure. The figure shows also the results obtained by Sellaro et al. [39] by using TiO_2 Nafion membrane, which represents the first attempt to perform this reaction in a photo-catalytic membrane reactor.

The reactor with C_3N_4/Nafion membrane showed a prevalent formation of alcohols (MeOH and EtOH) with a total production of 32.8 µmol $g_{catalyst}^{-1}$ h^{-1} and 47.6 µmol $g_{catalyst}^{-1}$ h^{-1} of total converted carbon at the feed molar ratio equal to 5 (Figure 8a). So far, this value resulted the highest among those reported in open literature up to date. In this work, C_3N_4-TiO_2/Nafion membrane reactor, instead, resulted in a greater production of alcohols (48.8 µmol $g_{catalyst}^{-1}$ h^{-1}) with a marked methanol formation (44.7 µmol $g_{catalyst}^{-1}$ h^{-1}) with respect to EtOH, at the same conditions. The system resulted

globally more performant than the previous one with a carbon converted/catalyst weight of 58.2 μmol $g_{catalyst}^{-1}$ h^{-1} and more selective toward MeOH (Figure 8b) obtaining 83.2 versus 53.6 of the C_3N_4/Nafion membrane reactor.

This might be also attributed to the heterojunction formation of C_3N_4 based materials, which usually enhances photocatalytic performance to CO_2 conversion, as widely discussed in literature.[40] The positive effect on the MeOH selectivity can be ascribed to the presence of TiO_2, as it can be found in Sellaro et al. [39]. In that case, the reaction was carried out with a H_2O/CO_2 feed molar ratio of 5 and 3 bar of pressure, with a contact time of ca. 2.1 s and the reaction resulted fully selective towards MeOH. Figure 9 shows the MeOH production per gram of catalyst and the reaction selectivity as a function of TiO_2 embedded in the Nafion membrane. As it can be clearly seen, the MeOH production increases with the TiO_2 content, passing from 17.9 when only C_3N_4 was embedded into Nafion membrane to 45 for 100% of TiO_2. The total converted carbon passes from ca. 45 when only C_3N_4 or TiO_2 was embedded into Nafion membrane to 60 micro-mol $g^{-1}_{catalyst}$ h^{-1} – one third more - for C_3N_4 - TiO_2 composite. The membrane reactor with C_3N_4-TiO_2 photocatalyst, results thus more performant than the other systems in terms of carbon converted, even though less selective toward MeOH.

In all the three photocatalytic reactors, MeOH, EtOH, HCHO and Acetone were the solely products, whereas we did not observe CO,CH_4 or H_2. The photocatalytic CO_2 reduction mechanism is very complex and various hypotheses were advanced on the formation of the various products deriving from CO_2. Generally, the compounds formed during the gaseous photocatalytic CO_2 reduction were CO and CH_4 whilst formic acid, formaldehyde and methanol were mainly observed during liquid phase runs. The absence of CH_4, CO and H_2 can probably be firstly attributed to a higher H_2O/CO_2 feed molar ratio. Secondly, the synergic effect of the use of membranes inside which the photocatalyst was embedded and a continuous flow mode reactor to carry out the reaction of CO_2 and H_2O leads to a faster removal of the formed products, which undergo a lower degree of reduction.44

Conclusions

In this work, CO_2 reduction was carried out in a continuous photocatalytic reactor with an exfoliated C_3N_4-TiO_2 loaded membrane, not reported up today in the literature, irradiated by UV light. The assets offered by the continuous operating mode of the membrane reactor were coupled with the use of an enhanced photocatalyst (C_3N_4-TiO_2) directly embedded in a dense polymer matrix. The effect of H_2O/CO_2 feed molar ratio, contact time and feed pressure on species production, reaction selectivity and converted carbon were investigated. Total converted carbon/catalyst weight ratio varied between 5 to 61 μmol $g_{catalyst}^{-1}$ h^{-1}, with the latter value obtained at an H_2O/CO_2 feed molar ratio of 5, 3 bar as feed pressure and 2 s as contact time with MeOH as the prevailing product.

Overall, alcohols production, most of which is MeOH, was promoted by a low contact time and high H_2O/CO_2 feed molar ratio as a result of the fast removal of the reaction mixture from the reaction volume exposed to UV light and, thus, with less promotion of oxidation and/or side reactions. On the contrary, the slow removal as well as the water defect caused a partial oxidation of MeOH and EtOH, favoring HCHO production. Feed pressure effect was specifically investigated for the first time in literature. At 5 bar, MeOH and HCHO resulted the unique products, with a lower amount of MeOH and a greater amount of HCHO with respect to the results obtained at 3 bar. This behavior could be attributed to a hindered desorption induced by the higher reaction pressure, which leads to partial oxidation reactions and, thus, to the formation of HCHO to the detriment of MeOH.

The comparison with other photocatalytic membrane reactors developed by us showed that the MeOH production increases with the TiO_2 content in the catalytic membrane, passing from 17.9 when only C_3N_4 was embedded into Nafion membrane to 45 for 100% of TiO_2. Membrane reactor with C_3N_4-TiO_2 photocatalyst, resulted more performant than the other systems in terms of carbon converted, even though less selective toward MeOH.

Acknowledgements

The research project PON 01_02257 "FotoRiduCO$_2$ - Photoconversion of CO$_2$ to methanol fuel", co-funded by MiUR (Ministry of University Research of Italy) with Decreto 930/RIC 09-11-2011 in the framework the PON "Ricerca e competitività 2007-2013", is gratefully acknowledged.

References

References

1 E. I. Koytsoumpa, C. Bergins, E. Kakaras, The CO_2 economy: Review of CO_2 capture and reuse technologies, *The Journal of Supercritical Fluids*, 2018, **132,** 3

2 http://www.captage-stockage-valorisation-CO_2.fr/en/principles-CO_2-reuse

3 S. Das, W. M. A. Wan Daud, A review on advances in photocatalysts towards CO_2 conversion, *RSC Advances*, 2014, **4**, 20856

4 J. W. Maina, C. Pozo-Gonzalo, L. Kong, J. Shutz, M. Hill, L. F. Dumee, Metal Organic Framework based catalyst for CO_2 conversion, *Materials Horizon*, 2017, **4(3)**, 345

5 A. Faunce, W. Lubitz, A. W. Rutherford, D. MacFarlane, G. F. Moore, P. Yang, D. G. Nocera, T. A. Moore, D. H. Gregory, S. Fukuzumi, K. B. Yoon, F. A. Armstrong, M. R. Wasielewski, S. Styring, Energy and environment policy case for a global project on artificial photosynthesis, *Energy and Environmental Science*, 2013,*6*, 695

6 K. Li, B. Peng, J. Jin, L. Zan, T. Peng, Carbon nitride nanodots decorated brookite TiO_2 quasi nanocubes for enhanced activity and selectivity of visible-light-driven CO_2 reduction. *Applied Catalysis B: Environmental*, 2017, **203**, 910

7 M. K. Hossain, A. R. Koirala, U. S. Akhtar, M. K. Song, K. B. Yoon, First Synthesis of Highly Crystalline, Hexagonally Ordered, Uniformly Mesoporous TiO_2–B and Its Optical and Photocatalytic Properties, *Chemistry of Materials,* 2015, **27, 19**, 6550

8 B. Elgh, N. Yuan, H. S. Cho, D. Magerl, M. Philipp, S. V. Roth, Kyung Byung Yoon, P. Müller-Buschbaum, O. Terasaki, A. E. C. Palmqvist, Controlling morphology, mesoporosity, crystallinity, and photocatalytic activity of ordered mesoporous TiO_2 films prepared at low temperature, *APL Materials*, 2014, **2**, 113313

9 M. Dilla, A. Mateblowski, S. Ristig, J. Strunk, Photocatalytic CO_2 Reduction under Continuous Flow High-Purity Conditions: Influence of Light Intensity and H_2O Concentration, *ChemCatChem*, 2017, **9**, 4345

10 E. Masolo, N. Senes, E. Pellicer, M. Dolors Baro, S. Enzo, M. I. Pilo, G. M., S. Garroni, Evaluation of the anatase/rutile phase composition influence on the photocatalytic performances of mesoporous TiO_2 powders, *International Journal of Hydrogen Energy*, 2015, **40**, 14483

11 C. Huang, R. Guo, W. Pan, J. Tang, W. Zhou, X. Liu, H. Qin, P. Jia, One-dimension TiO_2 nanostructures with enhanced activity for CO_2 photocatalytic reduction, *Applied Surface Science*, 2019, **464**, 534

12 P. Kar, S. Zeng, Y. Zhang, E. Vahidzadeh, A. Manuel, R. Kisslinger, K. M. Alam, U. K. Thakur, N. Mahdi, P. Kumar, K. Shankar, High rate CO_2 photoreduction using flame annealed TiO_2 nanotubes, *Applied Catalysis B: Environmental*, 2019, **243**, 522

13 Z. Sun, N. Talreja, H. Tao, J. Texter, M. Muhler, J. Strunk, J. Chen, Catalysis of Carbon Dioxide Photoreduction on Nanosheets: Fundamentals and Challenges, *Angew. Chem. Int. Ed*., 2018, **57**, 7610

14 K. Li, T. Peng, Z. Ying, S. Song, J. Zhang, Ag-loading on brookite TiO_2 quasi nanocubes with exposed {2 1 0} and {0 0 1} facets: activity and selectivity of CO_2 photoreduction to CO/CH_4, *Appl. Catal. B: Environ*., 2016, **180**, 130

15 C. Han, Y. Wang, Y. Lei, B. Wang, N. Wu, Q. Shi, Q. Li, In situ synthesis of graphitic- C_3N_4 nanosheet hybridized N-doped TiO_2 nanofibers for efficient photocatalytic H_2 production and degradation, Nano Research, 2015, **8**, 1199

16 L. Jiang, X. Yuan, G. Zeng, Z. Wu, J. Liang, X. Chen, L. Leng, H. Wang, H. Wang, Metal-free efficient photocatalyst for stable visible-light photocatalytic degradation of refractory pollutant. *Applied Catalysis B: Environmental*, 2018, **221** (Supplement C), 715

17 W.-J. Ong, L.-L. Tan, Y. H. Ng, S.-T. Yong, S.-P. Chai, Graphitic Carbon Nitride (g-C_3N_4)-Based Photocatalysts for Artificial Photosynthesis and Environmental Remediation: Are We a Step Closer To Achieving Sustainability? *Chemical Reviews*, 2016, **116 (12),** 7159

18 J. Wang, M. Li, M. Qian, S. Zhou, A. Xue, L. Zhang, Y. Zhao, W. Xing, Simple Synthesis of High Specific Surface Carbon Nitride for Adsorption-Enhanced Photocatalytic Performance, *Nanoscale Research Letters*, 2018, **13**, 248

19 Y. Wang, L. Li, Y. Wei, J. Xue, H. Chen, L. Ding, J. Caro, H. Wang, Water transport with ultralow friction through partially exfoliated g-C3N4 nanosheet membranes with self-supporting spacers, *Angew Chem Int Ed*., 2017, 56, 8974

20 J. Wang, M. Li, S. Zhou, A. Xue, Y. Zhang, Y. Zhao, J. Zhong, Q. Zhang, Graphitic carbon nitride nanosheets embedded in poly (vinyl alcohol) nanocomposite membranes for ethanol dehydration via pervaporation, *Separation and Purification Technology*, 2017,**188**, 24

21 K. Cao, Z. Jiang, X. Zhang, Y. Zhang, J. Zhao, R. Xing, S. Yang, C. Gao, F. Pan, Highly water-selective hybrid membrane by incorporating g-C3N4 nanosheets into polymer matrix, 2015, *Journal of Membrane Science,* **490**, 72

22 L.J. Fang, Y. H. Li, P.F. Liu, D.P. Wang, H. Zeng, X. Wang, H.G. Yang, Facile fabrication of large-aspect-ratio g-C_3N_4 nanosheets for enhanced photocatalytic hydrogen evolution, *ACS Sustainable Chemistry and Engineering*, 2017, **5**, 2039

23 X.G. Ma, Y.H. Lv, J. Xu, Y.F. Liu, R.Q. Zhang, Y.F. Zhu, A strategy of enhancing the photoactivity of g-C_3N_4 via doping of nonmetal elements: a first-principles study, *Journal of Physical Chemistry C*, 2012, **116**, 23485

24 X. Zhang, X. Xie, H. Wang, J. Zhang, B. Pan, Y. Xie, Enhanced photoresponsive ultrathin graphitic-phase C_3N_4 nanosheets for bioimaging, *Journal of American Chemical Society*, 2013, **135**, 18

25 X. Ding, J. Guo, X. Feng, Y. Honsho, J. Guo, S. Seki, P. Maitarad, A. Saeki, S. Nagase, D. Jiang, Synthesis of metallophthalocyanine covalent organic frameworks that exhibit high carrier mobility and photoconductivity. *Angewante Chemie Int. Ed*. 2011, **50**, 1289

26 X.Wang, S. Blechert, M. Antonietti, Polymeric Graphitic Carbon Nitride for Heterogeneous Photocatalysis, *ACS Catalysis*, 2012, **2**, 1596

27 J. Wen, J. Xie, X. Chen, X. Li, A review on g-C_3N_4-based photocatalysts, *Applied Surface Science,* 2017, **391**, 72

28 K. C. Crake, R. Christoforidis, B. Godin, A. Moss, S. Kafizas, J.R. Zafeiratos, C. Durrant, C. Petit, Titanium dioxide/carbon nitride nanosheet nanocomposites for gas phase CO_2 photoreduction under UV-visible irradiation, *Applied Catalysis B: Environmental*, 2019, **242**, 369

29 K. Dai, L. Lu, C. Liang, Q. Liu, G. Zhu, Heterojunction of facet coupled g-C3N4/surface-fluorinated TiO2 nanosheets for organic pollutants degradation under visible LED light irradiation, *Applied Catalysis B: Environmental*, 2014, 156–157, 331

30 J. Lv, J. Zhang, J. Liu, Z. Li, K. Dai, C. Liang, Bi SPR-Promoted Z‑ Scheme Bi_2MoO_6/CdS-Diethylenetriamine Composite with Effectively Enhanced Visible Light Photocatalytic Hydrogen Evolution Activity and Stability, *ACS Sustainable Chemistry and Engineering*, 2018, **6**, 696

31 Y. Huo, Y. Yang, K. Dai, J. Zhang, Construction of 2D/2D porous graphitic C_3N_4/SnS_2 composite as a direct *Z*-scheme system for efficient visible photocatalytic activity, *Applied Surface Science*, 2019, **481**, 1260

32 J. Yu, S. Wang, J. Low, W. Xiao, Enhanced photocatalytic performance of direct Z-scheme g-C_3N_4-TiO_2 photocatalysts for the decomposition of formaldehyde in air, *Physical Chemistry: Chemistry Physics*, 2013, **15**, 16883

33 X. Chen, J. Wei, R. Hou, Y. Liang, Z. Xie, Y. Zhu, X. Zhang, H. Wang, Growth of g- C_3N_4 on mesoporous TiO_2 spheres with High photocatalytic activity under visible light irradiation, *Applied Catalysis B: Environmental*, 2016, **188**, 342

34 M. Reli, P. Huo, M. Šihor, N. Ambrožová, I. Troppová, L. Matějová, J. Lang, L. Svoboda, P. Kuśtrowski, M. Ritz, P. Praus, K. Kočí, Novel TiO_2/C_3N_4 photocatalysts for photocatalytic reduction of CO_2 and for photocatalytic decomposition of N_2O, *Journal of Physical Chemistry A*, 2016, **120**, 8564

35 J. Yan, P. Li, H. Bian, H. Wu, S. Liu, Synthesis of a nano-sized hybrid C_3N_4/TiO_2 sample for enhanced and steady solar energy absorption and utilization, *Sustainable Energy Fuels*, 2017,**1**, 95

36 K. Dai, J. Lv, J. Zhang, G. Zhu, L. Gerng, C. Liang, Efficient visible-light- driven splitting of water into hydrogen over surface-fluorinated anatase TiO_2 nanosheets with exposed [001] facets/layered CdS-Diethylenetriamine nanobelts, *ACS Sustainable Chemistry and Engineering*, 2018, **6**, 12817

37 Z. Wang, J. Lv, J. Zhang, K. Dai, C. Liang, Facile synthesis of Z-scheme $BiVO_4$/porous graphite carbon nitride heterojunction for enhanced visible-light-driven photocatalyst, *Applied Surface Science*, 2018, **430**, 595

38 Y. Huo, J. Zhang, K. Dai, Q. Li, J. Lv, G. Zhu, All-solid-state Z-scheme porous g-C_3N_4/Sn_2S_3-DETA heterostructure photocatalyst with enhanced performance in photocatalytic CO_2 reduction, *Applied Catalysis B: Environmental*, 2019, **241**, 528

39 M. Sellaro, M. Bellardita, A. Brunetti, E. Fontananova, L. Palmisano, E. Drioli, G. Barbieri, CO_2 conversion in a photocatalytic continuous membrane reactor, RSC Advances, 2016, **6**, 67418

40 F. R. Pomilla, A. Brunetti, G. Marcì, E. I. Garcia-Lopez, E. Fontananova, L. Palmisano, G. Barbieri, CO_2 to liquid fuels: photocatalytic conversion in a continuous membrane reactor, *ACS Sustainable Chemistry and Engineering*, 2018, **6**, 8743

41 D. Shi, Y. Feng, S. Zhong, Photocatalytic conversion of CH_4 and CO_2 to oxygenated compound over Cu/CdS-TiO_2/SiO_2 catalyst, *Catalysis Today*, 2004, **98**, 505

42 Y. Hori, R. Takahashi, Y. Yoshinami, A. Murata, Electrochemical reduction of CO at copper electrode, *Journal of Physical Chemistry B*, 1997, **101**, 7075

43 Z. Sun, H. Wang, Z. Wu, L. Wang, g-C3N4 based composite photocatalysts for photocatalytic CO_2 reduction, *Catalysis Today*, 2018, **300**, 160

44 M. Bellardita, A. Di Paola, E. García-López, V. Loddo, G. Marcì, L. Palmisano, Photocatalytic CO_2 Reduction in Gas-Solid Regime in the Presence of Bare, SiO_2 Supported or Cu-Loaded TiO_2 Samples, *Current Organic Chemistry*, 2013, **17**, 2440.

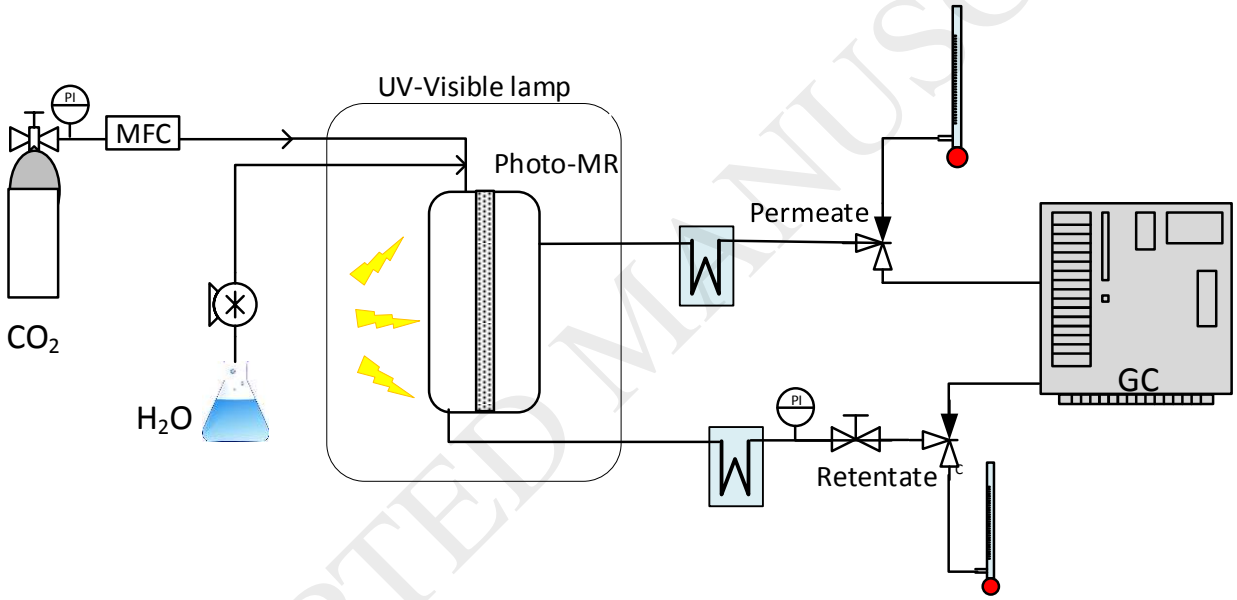

Figure 1. Scheme of photocatalytic membrane reactor setup.

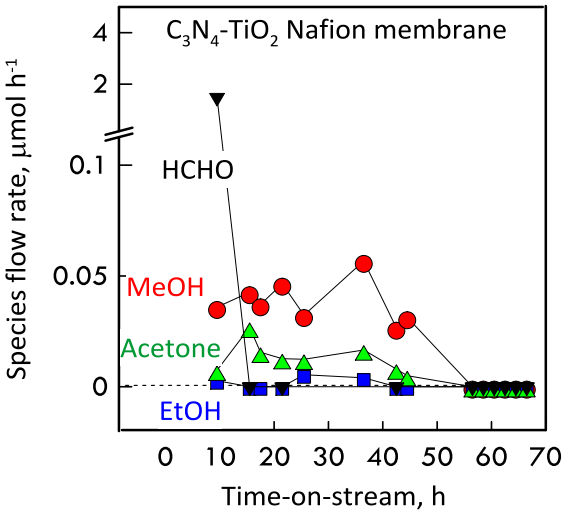

Figure 2 - Cleaning of the C_3N_4-TiO_2 loaded Nafion membrane.

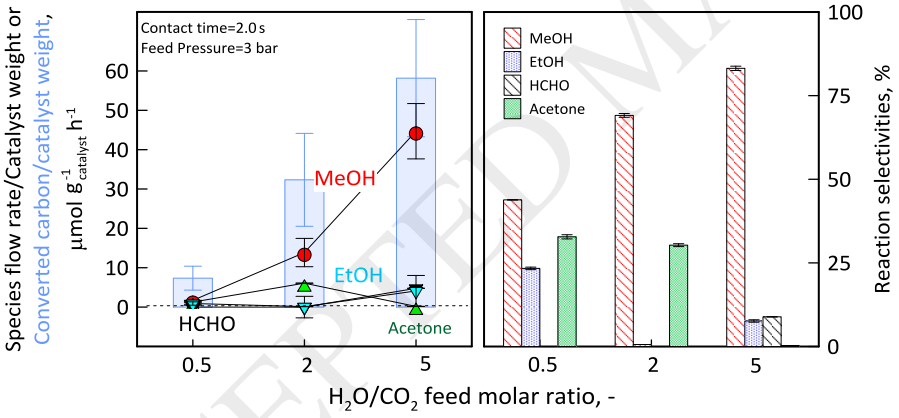

Figure 3 – Species flow rate/catalyst weight and reaction selectivity of the reaction products as a function of H_2O/CO_2 feed molar ratio at a contact time of 2 s.

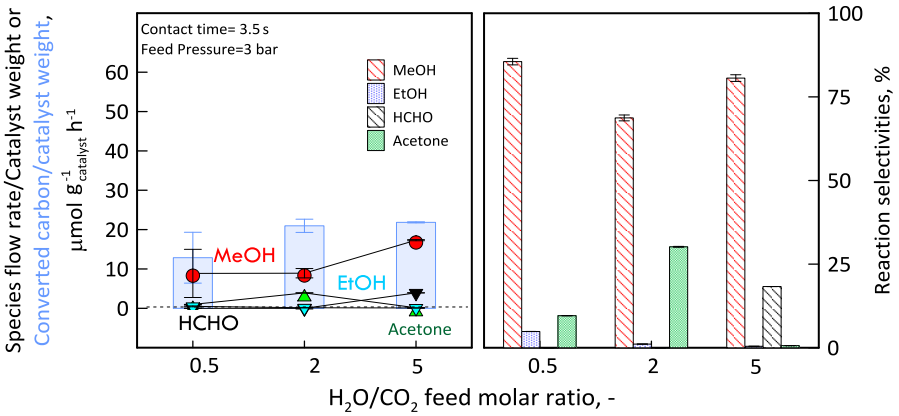

Figure 4 - Species flow rate/catalyst weight and reaction selectivity of the reaction products as a function of H_2O/CO_2 feed molar ratio at a contact time of 3.5 s.

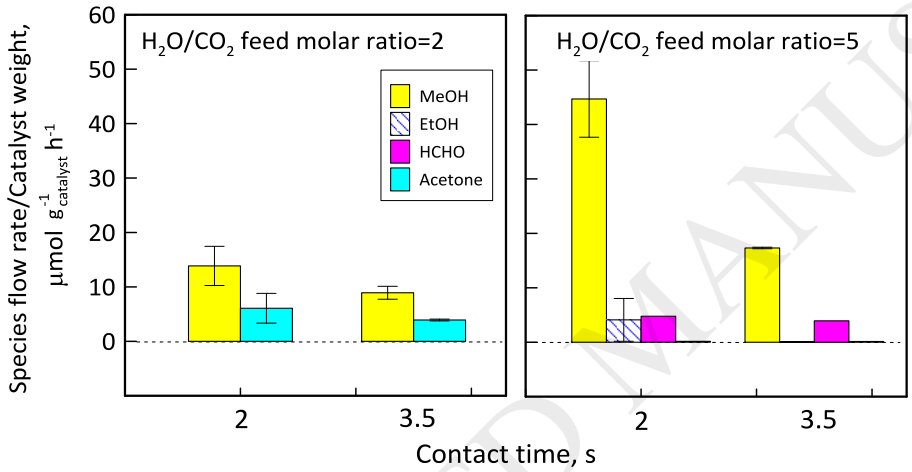

Figure 5 – Species flow rate/catalyst weight of the products as a function of the contact time at H_2O/CO_2 feed molar ratio of 2 and 5.

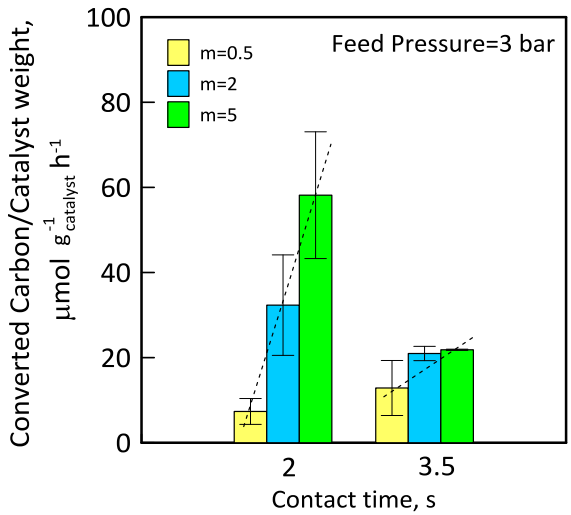

Figure 6 – Converted Carbon/catalyst weight as a function of the contact time at different H_2O/CO_2 feed molar ratios (indicated as "m").

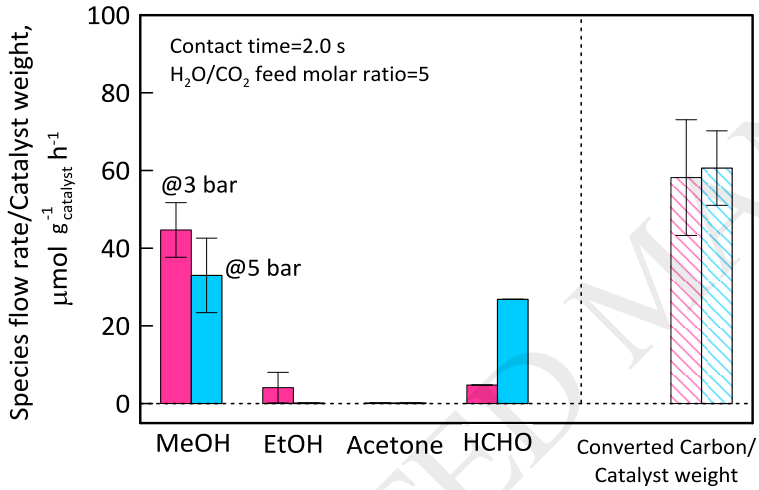

Figure 7 – Species flow rate/ and Converted Carbon / catalyst weight at 3 and 5 bar.

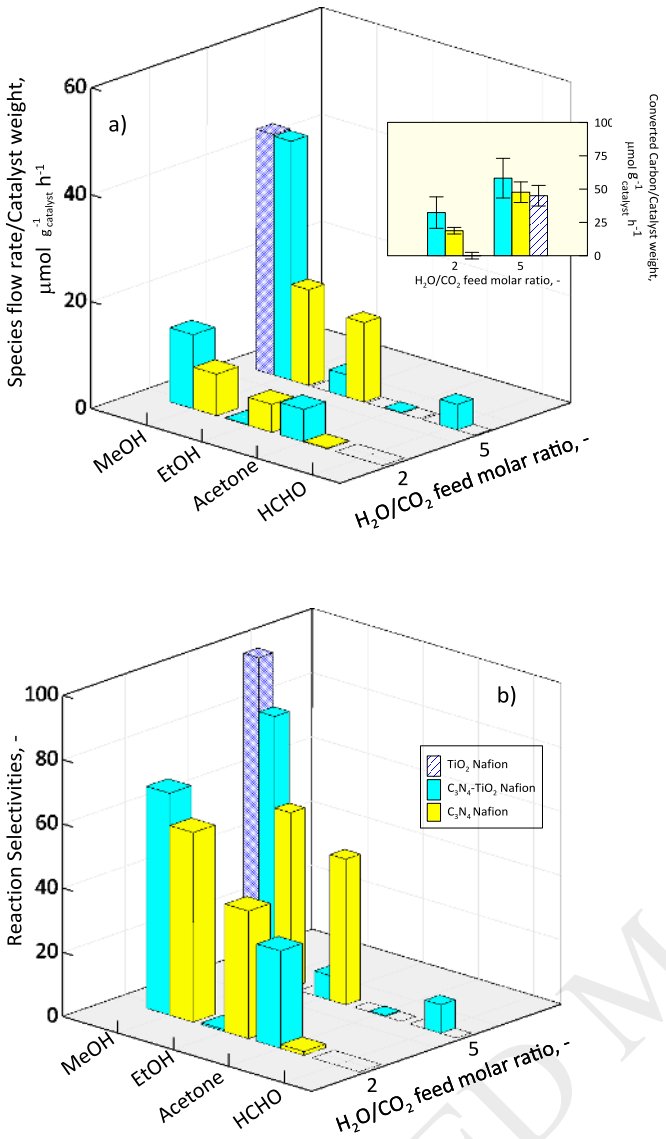

Figure 8 – Comparison of a) species flow rate/catalyst weight and b) reaction selectivity towards the reaction products at H_2O/CO_2 feed molar ratios of 2 and 5 for C_3N_4-TiO_2/Nafion (light-blue bars) and C_3N_4/Nafion (yellow bars) and TiO_2/Nafion (dotted blue bars) photocatalytic membranes. Reaction pressure=3 bar and contact time=2.0 s. The inset shows the converted carbon on catalyst weight at the same conditions.

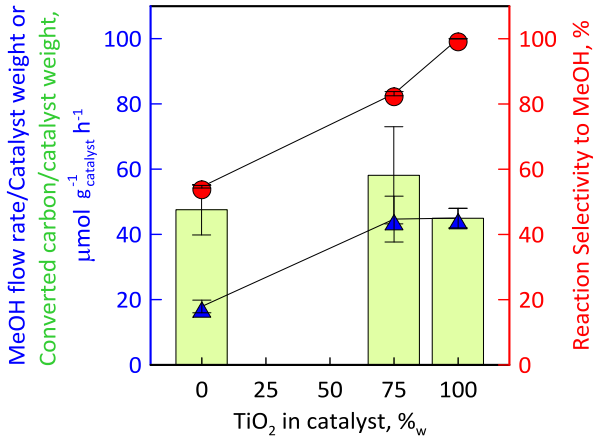

Figure 9 – MeOH flow rate/catalyst weight (filled in blue triangle over blue left axis) and reaction selectivity towards MeOH (filled in red circle over red right axis) and converted carbon (green bars) for C_3N_4-TiO_2-Nafion (blue bars)as a function of the TiO_2 percentage in the catalyst embedded in the photocatalytic membrane. Reaction pressure= 3 bar, H_2O/CO_2 feed molar ratio= 5 and contact time=2.0 s.